CHIN. PHYS. LETT. Vol. 35, No. 9 (2018) 095201

# Electron Dynamics and Characteristics of Attosecond Electromagnetic Emissions in Relativistic Laser-Plasma Interactions *

Yi-Ying Wu(吴奕莹)[1], Quan-Li Dong(董全力)[1,2**], Zhao-Hua Wang(王兆华)[2], Ping Liu(刘苹)[1], Cheng-Zhen Wang(王成朕)[1], Yi-Hui Zhang(张以辉)[1], Zheng-Ming Sheng(盛政明)[3,4], Jie Zhang(张杰)[4,5]

[1]*School of Physics and Optoelectronics Engineering, Ludong University, Yantai 264025*
[2]*Beijing National Laboratory of Condensed Matter Physics, Institute of Physics, Chinese Academy of Sciences, Beijing 100190*
[3]*School of Physics and Astronomy, Shanghai Jiao Tong University, Shanghai 200240*
[4]*Innovative Collaboration Center of IFSA, Shanghai Jiao Tong University, Shanghai 200240*
[5]*University of Chinese Academy of Sciences, Beijing 100864*

(Received 20 March 2018)

*Generation of attosecond electromagnetic (EM) pulses and the associated electron dynamics are studied using particle-in-cell simulations of relativistic laser pulses interacting with over-dense plasma foil targets. The interaction process is found to be so complicated even in the situation of utilizing driving laser pulses of only one cycle. Two electron bunches closely involved in the laser-driven wavebreaking process contribute to attosecond EM pulses through the coherent synchrotron emission process whose spectra are found to follow an exponential decay rule. Detailed investigations of electron dynamics indicate that the early part of the reflected EM emission is the high-harmonics produced through the relativistic oscillating mirror mechanism. High harmonics are also found to be generated through the Bremsstrahlung radiation by one electron bunch that participates in the wavebreaking process and decelerates when it experiences the local wavebreaking-generated high electrostatic field in the moving direction.*

*PACS: 52.38.Kd, 52.25.Os, 52.25.Tx* DOI: 10.1088/0256-307X/35/9/095201

Intense attosecond pulses attract great interest in their many potential applications such as selecting quantum paths in strong field processes,[1] studying the photoionization or dissociation process of chemical molecular,[2,3] and performing photoelectron holography.[4] Coherent attosecond pulses with frequencies located in the extreme ultraviolet (XUV) and x-ray ranges can be produced through various mechanisms of the high-order harmonic generation (HHG), the interesting nonlinear process occurring when electrons are exposed to an intense laser field.[5] Three emission mechanisms have been identified to contribute to the HHG in the interaction of ultrashort relativistic laser pulses with dense plasmas. They are the coherent wake emission (CWE),[6–8] the coherent synchrotron emission (CSE)[9–12] and the emission or reflection from the relativistic oscillating mirror (ROM).[13–16]

The CWE mechanism is a conversion process of the plasma coherent oscillations into the electromagnetic (EM) emission, which is demonstrated theoretically and experimentally by Quéré *et al.*[7] A transient phase match between the EM field and the plasma with a density gradient leads to the emission at harmonics up to the plasma frequency. These plasma waves are excited in the wake of attosecond electron bunches and sweep across the density gradient.[7] The basic physical process of the harmonic generation from the ROM is the Doppler frequency-upshifted reflection of the driving laser from the collective oscillations of a plasma surface. Its harmonic spectrum has a fast intensity decay versus the harmonic order as $I(n) \propto n^{-8/3}$.[10,13–15] When compact dense electron nanobunches interact with the intense laser, their strong transverse acceleration by the intense magnetic component produces high harmonics and the attosecond pulses of XUV. Such an HHG mechanism is identified as the CSE by Brügge *et al.*[9] Both theoretical[9,10] and experimental[11] studies find that the spectrum of CSE harmonics has a slow decay scaling as $I(n) \propto n^{-4/3} \sim n^{-6/5}$, indicating a higher conversion efficiency. The ROM and CSE usually occur in the relativistic regime with $a_0 \geqslant 1$, while the CWE is predominant at moderately relativistic intensities $a_0 \sim 1$.[9,13,15]

A complicated generation process of attosecond XUV pulses is reported as the wavebreaking associated transmitted emission (WTE) by Chen *et al.* in the study of a relativistic laser pulse irradiating on an overdense plasma surface.[17] It is found that the strong wavebreaking process of the plasma generates XUV pulses in the transmitted direction. However, the detailed process of the EM pulse generation associated with the wavebreaking is not discovered in that work. A phenomenon-phenomenon connection does not naturally bring out the underlying physical rules. In this Letter, we correlate the dynamics of wavebreaking-involved energetic electrons to the EM pulse production, describe their characteristics, and distinguish different generation mechanisms.

*Supported by the National Natural Science Foundation of China under Grant No 11674146, and the National Basic Research Program of China under Grant No 2013CBA01500.
**Corresponding author. Email: qldong@iphy.ac.cn
© 2018 Chinese Physical Society and IOP Publishing Ltd

To perform the simulations, we use a relativistic particle-in-cell (PIC) code dealing with one dimension and three velocities (1D3V). A linearly polarized laser pulse with a Gaussian temporal profile is launched from the left boundary of the target in the normal direction. The normalized strength of the laser field is taken as $a_0 = eE_L/m_e\omega_L c = 20$, corresponding to an intensity of $I = 8.56 \times 10^{20}\,\mathrm{W/cm^2}$, where $\lambda_L = 0.8\,\mu\mathrm{m}$, $E_L$, and $\omega_L$ are the amplitude and the frequency of the laser pulse, $e$ and $m_e$ are the electron charge and mass, and $c$ is the velocity of light in a vacuum. The full width at half maximum (FWHM) of the driving laser $L_{FWHM} \approx 1.18\,\mathrm{fs}$. The simulation box has a length of $6.15\lambda_L$ along the $x$ direction with the region between $5\lambda_L$–$5.15\lambda_L$ occupied by the plasma foil target. One wavelength is divided into 2000 cells with each cell filled with 100 macroparticles. The electron density $n_e = 100n_c$, with $n_c = m_e\omega_L^2/4\pi e^2$ as the critical density for the used wavelength. In simulations, the initial electron temperature is assumed to be 100 eV and the ions are immobile.

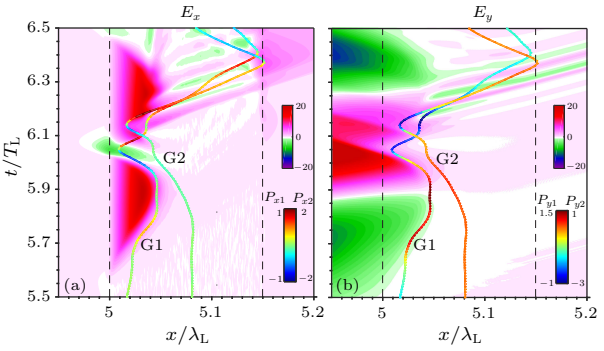


**Fig. 1.** (Color online) (a) The time-spatial distribution of the longitudinal electric field $E_x$, overlaid with the trajectories of two typical electrons from nanobunches marked as G1 and G2. The color of the trajectories represents the $x$-component of momentum ($P_{x1}$ and $P_{x2}$) of the two typical electrons. (b) The time-spatial distribution of the transverse electric field $E_y$, overlaid with the trajectories of the same two electrons in (a). The color of the trajectories represents the $y$-component of momentum ($P_{y1}$ and $P_{y2}$). The black dashed lines indicate the boundary of the plasma target.

The spatial and temporal distributions of the $x$ and $y$ components of the electric field are shown in Figs. 1(a) and 1(b), respectively. When the driving laser pulse is incident on the plasma surface, the strong ponderomotive force $F_p = -e^2\nabla|E_L|^2/4\gamma m_e\omega_L^2$ with $\gamma = \sqrt{1+(v/c)^2}$ smoothly compresses the electron layer and pushes it away from the ion background, setting up a giant positive (pointing to the $x$-direction) electrostatic field $E_x$ shown in Fig. 1(a). The value of $F_p$ has a frequency of $2\omega_L$, between the two time intervals of positive $E_x$ there appears a negative $E_x$ of a very narrow time interval, which is formed by those previously accelerated electrons when $E_x$ is positive. The transverse electric field $E_y$ presents drastic variations in amplitude, as shown in Fig. 1(b). Unlike $E_x$, $E_y$ is distributed across the whole foil target, as well as in the space around the target. Overlaid on the spatial and temporal distributions of $E_x$ and $E_y$ are typical trajectories of two electrons from different groups involved in the generation of attosecond EM pulses, i.e., the high-harmonic emissions. The color of the trajectory lines presents electron momentum in the $x$ direction (Fig. 1(a)) and in the $y$ direction (Fig. 1(b)).

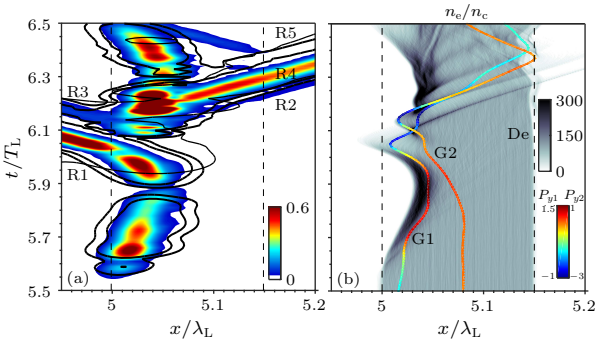


**Fig. 2.** (Color online) The electromagnetic emission and the density. (a) The spatial and temporal distribution of the attosecond pulses. The colorful patches, bold solid black lines, and thin solid black lines represent the attosecond pulses ($E_y$) whose frequency ranges are $60\omega_L$–$100\omega_L$, $30\omega_L$–$60\omega_L$, and $10\omega_L$–$30\omega_L$, respectively. (b) The spatial and temporal distribution of the electron density $n_e$, which is overlaid by the two electron trajectories with the color represents their transverse momentum $P_y$, as shown in Fig. 1.

After the low-frequency components are filtered out, attosecond pulses consisting of high order harmonics are obtained. The spatial and temporal distribution of their $E_y$ components is shown in Fig. 2(a). The colorful patches, bold lines, and thin lines represent the frequency ranges $60\omega_L$–$100\omega_L$, $30\omega_L$–$60\omega_L$, and $10\omega_L$–$30\omega_L$, respectively. Those separated attosecond pulses are marked by R$i$ ($i$ = 1–5) with pulses R1 and R3 being in the reflection and others in the transmission. The attosecond pulses R$i$ ($i$ = 1–5) have frequency ranges $10\omega_L$–$100\omega_L$, $60\omega_L$–$100\omega_L$, $10\omega_L$–$100\omega_L$, $10\omega_L$–$100\omega_L$, and $10\omega_L$–$60\omega_L$, respectively.

The S-transform (ST)[18] is performed to produce the time-frequency spectrum of the whole EM emissions respectively in the reflection and in the transmission. Each attosecond pulse is then separated from the time-frequency spectrum and the corresponding spectra are shown in Fig. 3. The generalized Gaussian window is used in the ST operation for its advantages of the flexibility in the window width and amplitude, and the algorithm is perfectly invertible.[18] In the reflected direction (Fig. 3(a)), the red and blue solid lines are the spectra of the attosecond pulses marked as R1 and R3 in the time intervals of 5.95 fs–6.05 fs and 6.10 fs–6.15 fs, respectively. The two lines can be fitted by an exponential function as $\exp(-n/A + B)$, with $(A, B) = (9.8, 2.8)$ for R1 and (8, 0.5) for R3. This is the approximated formula for the spectral distribution of the synchrotron radiation with $A$ as a function of the electron's kinetic energy and the magnetic strength is experienced. The claim that R1 and R3

are generated by the CSE process is also supported by the dynamics of those emission-involved electrons, which are shown in Fig. 4 and will be discussed in the following. The other three lines, the black, purple, and green solid lines in Fig. 3(a) are the spectra of the emission in the time intervals of 5.70 fs–5.90 fs, 6.15 fs–6.30 fs, and 6.30 fs–6.50 fs, respectively. The black line spectrum takes place when the plasma density is being compressed from the vacuum-plasma interface into the inside target as shown in Fig. 2(b). It declines very quickly as the harmonic order increases. The slopes of the purple line and the green line have the similar trend, but the amplitude vibration of the green line is larger. As a comparison, the spectra of the formula $I(n) \propto n^{-8/3}$ are plotted as the dashed line, which are derived to show the characteristics of the emission produced by the ROM mechanism.[10,13–15] The complicated structure of the purple (green) line spectrum indicates the violent variation of the laser-plasma interface, and makes it difficult to identify its generation mechanism. However, the black line spectrum is taken when the moving laser-plasma interaction surface is smooth, thus it can be attributed to the laser reflection on the ROM. Its intensity scaling curve deviates from the theoretical prediction, which may be understood in that the theory takes considerations of interaction in the whole laser cycle.[13]

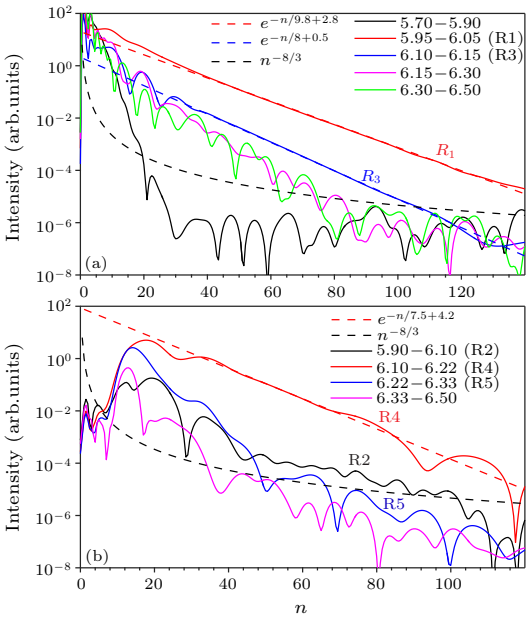


**Fig. 3.** (Color online) The spectra of each attosecond pulse R$i$ ($i$ = 1–5) in the reflection (a) and the transmission (b), respectively. The spectra of the high harmonics in other time intervals are also given. The dashed lines shown together are the theoretical spectral distribution of the synchrotron radiation $I(n) \propto \exp(-n/A + B)$ and the high-harmonic emission from the ROM $I(n) \propto n^{-8/3}$.

Figure 3(b) shows the spectra of the emissions in the transmission with the time intervals of 5.90 fs–6.10 fs (black, R2), 6.10 fs–6.22 fs (red, R4), 6.22 fs–6.33 fs (blue, R5), and 6.33 fs–6.50 fs (purple), respectively. The spectrum of the formula $I(n) \propto n^{-8/3}$ is also given. No line from the four time intervals has the trend of $I(n) \propto n^{-8/3}$. It is obvious that R2 and R5 are not produced through the ROM mechanism, as they originate deeply in the plasmas where the laser pulse does not exist. The red solid line (R4) is fitted by the exponential function with $(A, B) = (7.5, 4.2)$. The generation mechanisms of the attosecond pulses can be distinguished by analyzing the dynamics of electrons involved in the attosecond radiation generation processes.

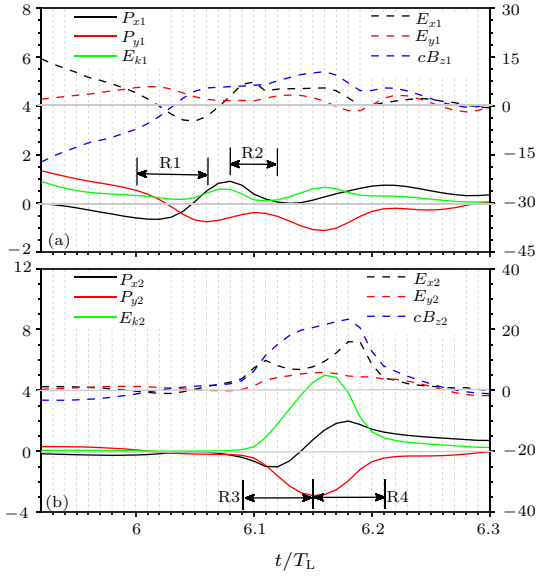


**Fig. 4.** (Color online) Dynamics of the electrons and their experienced electric and magnetic field. (a) Momentum, kinetic energy, experienced electric, and magnetic fields of/by electrons in G1. (b) The same as (a) but for electrons in G2.

Figure 4 gives the temporal evolutions of the two typical electrons' momentum and the EM field they experienced. One electron (in Fig. 4(a)) is from the group involved in the production of the attosecond pulses R1 and R2 (G1 in Fig. 2(b)). The other (in Fig. 4(b)) is from the group that emits R3 and R4 (G2 in Fig. 2(b)). Electrons of G1 originally in the depth of the target are accelerated in the negative $x$ direction by the positive field of $E_x$ as indicated by its trajectory and the increasing negative $P_{x1}$. This process ends at the time $t = 6.02T_L$. During the same period, the positive fields of $E_y$ and $B_z$ change the signs of $P_{y1}$, and $P_{y1}$ is firstly decelerated to zero at $t = 6.02T_L$ and then accelerated to its highest value at $t = 6.06T_L$. The electron trajectory is also modified. During this process in the time interval between $t = 6.00T_L$ and $t = 6.06T_L$, the electron is accelerated perpendicular to its velocity, resulting in an attosecond EM pulse R1 through the synchrotron radiation process. The coherence of R1 stems from the simultaneous short-time strong interactions of G1 electrons with the laser field. Around the time $t = 6.05T_L$, electrons of G1 experience the narrow-period negative $E_x$, during which interaction process, they begin to return to the inside target. At the time $t = 6.10T_L$, the first electron

group G1 crosses the trajectory of the other electron group G2 in opposite directions and a density spike is formed, as shown in Fig. 2(b), indicating that the wavebreaking takes place. After that, the density of the target begins to have violent oscillations and experiences multiple wavebreakings. The attosecond pulse R2 is the emission generated in the first wavebreaking during the time interval of $6.08T_{\rm L}$–$6.12T_{\rm L}$. From Fig. 4(a), it can be seen that the G1 electron loses its energy and momentum to the EM pulse R2 in its propagating direction, meaning that the Bremsstrahlung radiation dominates in the R2 generation process.

G2 is accelerated rapidly in the negative $x$ direction when the first wavebreaking takes place at $t \sim 6.10T_{\rm L}$. When they enter the laser field, the Lorentz force $E_x + v_y B_z$ decelerates them in the negative $x$ direction. During the same period, the laser magnetic field $B_z$ bends the G2 electron' trajectory into the $y$ direction, so that the Lorentz force $E_y - v_x B_z$ accelerates electrons to higher $|P_{y2}|$ in the negative $y$ direction. The attosecond EM pulse R3 is then produced in the reflection by the CSE process during the time interval between $t = 6.09T_{\rm L}$ and $6.15T_{\rm L}$. However, as the $x$-component of the Lorentz force $E_x + v_y B_z$ continues its exertions, electrons of G2 change in their propagation direction and return into the over-dense plasma. The $y$-component of the Lorentz force $E_y - v_x B_z$ begins to decelerate them in the negative $y$ direction and produces the EM pulse R4 through the CSE process.

When the laser pulse consists of multi cycles, a train of attosecond EM pulses is produced. All of the generation mechanisms of ultrashort XUV pulses mix together during the intense laser-plasma interaction. Interferences between attosecond pulses present on the spectra as fine structures. Chen *et al.* also investigated the effects of the density gradient of plasma foil targets and those of multi dimensions on the XUV pulse generation.[17]

In summary, the electron dynamics and the associated generation of attosecond EM pulses have been studied with the wavebreaking process when one intense laser pulse normally irradiates on a dense plasma foil target. Two distinct electron bunches closely related to the wavebreakings are observed to emit attosecond pulses in both the reflection and the transmission. The attosecond pulses are produced through the CSE mechanism when the compact electron nanobunches react to the laser field. The high harmonic generation by reflecting from the ROM is also observed in the early interaction process. However, the surface is then distorted by the following wavebreakings. The Bremsstrahlung radiation process presents itself when the electron bunch participate in the wavebreaking, during which the locally formed electrostatic field decelerates those electrons in their propagation direction. The present work is helpful for realizing the complicated generation process of the high harmonics or the attosecond EM pulse in intense laser-plasma interactions. Even in the situation of using driving laser pulses of only one cycle, several mechanisms are observed to have their rules.

## References


[1] Kenneth J S, Mette B G et al 2004 *Phys. Rev. Lett.* **92** 23003

[2] Sansone G, Kelkensberg F, Pérez-Torres J F, Morales F, Kling M F, Siu W, Ghafur O, Johnsson P, Swoboda M, Benedetti E, Ferrari F, Lépine F, Sanz-Vicario J L, Zherebtsov S, Znakovskaya I, L'Huillier A, Ivanov M Y, Nisoli M, Martin F and Vrakking M J J 2010 *Nature* **465** 763

[3] Mauritsson J, Gaarde M B and Schafer K J 2005 *Phys. Rev.* A **72** 13401

[4] Chen L Y, Huang C, Zhu X S, Lan P F and Lu P X 2014 *Opt. Express* **22** 20421

[5] Carrera J J, Tong X M and Chu S I 2006 *Phys. Rev.* A **74** 23404

[6] Borot A, Malvache A, Chen X W, Jullien A, Geindre J P, Audebert P, Mourou G, Quéré F and Lopez-Martens R 2012 *Nat. Phys.* **8** 416

[7] Quéré F, Thaury C, Monot P, Dobosz S, Martin P, Geindre J P and Audebert P 2006 *Phys. Rev. Lett.* **96** 125004

[8] George H, Quéré F, Thaury C, Bonnaud G and Martin P 2009 *New J. Phys.* **11** 113028

[9] Brügge D and Pukhov A 2010 *Phys. Plasmas* **17** 033110

[10] Dromey B, Rykovanov S, Yeung M, Hörlein R, Jung D, Gautier D C, Dzelzainis T, Kiefer D, Palaniyppan S, Shah R, Schreiber J, Ruhl H, Fernandez J C, Lewis C L S, Zepf M and Hegelich B M 2012 *Nat. Phys.* **8** 804

[11] Dromey B, Cousens S, Rykovanov S, Yeung M, Jung D, Gautier D C, Dzelzainis T, Kiefer D, Palaniyppan S, Shah R, Schreiber J, Fernandez J C, Lewis C L S, Zepf M and Hegelich B M 2013 *New J. Phys.* **15** 015025

[12] Cousens S, Reville B, Dromey B and Zepf M 2016 *Phys. Rev. Lett.* **116** 083901

[13] Baeva T, Gordienko S and Pukhov A 2006 *Phys. Rev.* E **74** 46404

[14] Dromey B, Zepf M, Gopal A, Lancaster K, Wei M S, Krushelnick K, Tatarakis M, Vakakis N, Moustaizis S, Kodama R, Tampo M, Stoeckl C, Clarke R, Habara H, Neely D, Karsch S and Norreys P 2000 *Nat. Phys.* **2** 449

[15] Pukhov A, Brügge D and Kostyukov I 2010 *Plasma Phys. Control. Fusion* **52** 124039

[16] Quéré F, Thaury C, Geindre J P, Bonnaud G, Monot P and Martin P 2008 *Phys. Rev. Lett.* **100** 095004

[17] Chen Z Y, Cherednychek M and Pukhov A 2016 *New J. Phys.* **18** 063014

[18] Stockwell R G, Mansinha L and Lowe R P 1996 *IEEE Trans. Signal Process.* **44** 998